Anal. Chem. **2005,** *77,* 3479−3487

In Situ Spatial and Time-Resolved Studies of Electrochemical Reactions by Scanning Transmission X-ray Microscopy

Daniel Guay,[†] Jacob Stewart-Ornstein,[‡] Xuerong Zhang,[‡] and Adam P. Hitchcock*[,‡]

Centre Énergie, Matériaux et Télécommunications, Institut National de la Recherche Scientifique, Varennes, QC, Canada J3X 1S2, and Department of Chemistry and Brockhouse Institute for Materials Research, McMaster University, Hamilton, ON, Canada L8S 4M1

The first in situ measurements with scanning transmission X-ray microscopy (STXM) of an active electrochemical cell are reported. An electrochemical wet cell, consisting of an electrodeposited polyaniline thin film on a thin Au film covered by an overlayer of 1 M HCl solution sitting between two X-ray transparent silicon nitride windows, was assembled. X-ray absorption images and spatial and time-resolved spectra of this system under potential control were examined using the beamline 5.3.2 STXM at the Advanced Light Source. The chemical state of the polyaniline film was reversibly converted between reduced (leucoemeraldine) and oxidized (emeraldine chloride) states by changing the applied potential. The electrochemical changes were monitored by spatially resolved C 1s and N 1s X-ray absorption spectroscopy and chemical-state selective imaging. Comparison of differences between images at two energies at different potentials provided electrochemical contrast with a resolution better than 50 nm, thereby monitoring that component of the polyaniline film that was electrochemically active. Kinematic studies in the subsecond regime are demonstrated.

Electrochemical processes on a submicrometer scale are important in a wide variety of applications, including biosensors[1,2] and energy storage, including batteries[3,4] and fuel cells,[5] and display devices.[6,7] To optimize these systems, it is useful to have access to experimental techniques capable of studying chemical structure at the submicrometer scale, while the system is under potential control. Synchrotron-based scanning transmission X-ray microscopy (STXM) is able to measure images and spectra through a few micrometers of aqueous solution with a lateral resolution better than 50 nm.[8−12] The photon energy-dependent contrast in these images arises from difference in the near edge X-ray absorption fine structure (NEXAFS)[13] features of the chemical species present. Image sequences, which track changes in optical density with energy, can be analyzed to generate quantitative maps of the chemical species involved. Thus, STXM has the potential to measure active electrochemical systems under potential control and thus assist in development of improved technologies involving electrochemistry or applied electrical fields. However, to date there have not been any published reports of in situ electrochemical studies using STXM, in part because it is a relatively new analytical technique and in part because there are significant challenges to realize the experiment given the spatial and environmental constraints of the microscope. Reversible and irreversible electrode processes as well as electrolyte, anion, and cation transport issues could be studied under potential control, if a set of cells and measurement protocols suitable for in situ electrochemical control could be developed. Here we report the first demonstration of in situ electrochemical scanning transmission X-ray microscopy.

Over the years, most studies to characterize electrode materials have been realized ex situ, in conditions where the electrode is dissembled from the electrochemical cell and the control of the electrode potential is lost. Obviously, the conditions prevailing during these ex situ measurements are different from those relevant to the electrochemical cell, where the electrode is under potential control and immersed in an electrolyte. While these ex situ studies have given a wealth of information on the electrode material and on the processes occurring at the solid−liquid interface, there has been an increasing tendency over the last years to develop procedures and experimental diagnostics to study

* To whom correspondence should be addressed. E-mail: aph@mcmaster.ca.
† Institut National de la Recherche Scientifique.
‡ McMaster University.

(1) Zhang, S.; Wright, G.; Yang, Y. *Biosens. Bioelectron.* **2000**, *5*−*6*, 273−82.
(2) Kerman, K.; Kobayashi, M.; Tamiya, E. *Meas. Sci. Technol.* **2004**, *15*, R1−R11.
(3) Winter, M.; Besenhard, J. O.; Spahar, M. E. Novak, P. *Adv. Mater.* **1998**, *10* 725−763.
(4) van Schalkwijk, W. A.; Scrosati, B. *Advances in Lithium Ion Batteries*; Kluwer Academic/Plenum: New York, 2000.
(5) Brandon, N. P.; Skinner, S.; Steele, B. C. H. *Ann. Rev. Mater. Res.* **2003**, *33*, 183−213.
(6) Trivedi, D. C. Polyanilines. In *Handbook of Organic Conductive Molecules and Polymers*; Nalwa, H. S., Ed.; Wiley: New York, 1997; Chapter 12.
(7) Somani, P. R.; Radhakrishnan, S. *Mater. Chem. Phys.* **2003**, *77*, 117−133.
(8) Ade, H. In *Experimental Methods in the Physical Sciences*; Samson, J. A. R., Ederer, D. L., Eds.; Academic Press: New York, 1998; Vol. 32, p 225,
(9) Ade, H.; Urquhart, S. G. In *Chemical Applications of Synchrotron Radiation*; Sham, T. K., Ed.; World Scientific Publishing: Singapore, 2002.
(10) Jacobsen, C.; Wirick, S.; Flynn, G.; Zimba, C. *J. Microsc.* **2000**, *197*, 173−184.
(11) Hitchcock, A. P.; Morin, C.; Heng, Y. M.; Cornelius, R. M.; Brash, J. L. *J. Biomater. Sci., Polym. Ed.* **2002**, *13*, 919−938.
(12) Morin, C.; Hitchcock, A. P.; Cornelius, R. M.; Brash, J. L.; Scholl, A.; Doran, A. *J. Electron. Spectrosc.* **2004**, *78*, 137−140.
(13) Stöhr, J. *NEXAFS Spectroscopy*; Springer Tracts in Surface Science 25; Springer-Verlag: Berlin, 1992.

10.1021/ac048077j CCC: $30.25
Published on Web 04/15/2005

electrified interfaces in situ.[14] If the experimental conditions can be achieved, STXM could be used to perform in situ characterization of electrochemical process by measuring images (5−60 s), spectra (1−10 s), or even simply watching the change in X-ray response with millisecond sampling as the electrode potential is varied.

A number of in situ electrochemical characterization methods are currently available. Many in situ optical techniques are used such as ellipsometry and vibrational spectroscopies.[15] In situ electrochemical STM and AFM[16] provide unprecedented spatial resolution (atomic resolution) on some carefully chosen systems. However, scanning probe techniques lack the chemical specificity necessary to distinguish between various elements and various chemical states (oxidation state) of the same element. In situ electrochemical X-ray diffraction[17−19] is useful to study phase transformations in electrode materials when the electrode potential is varied. However, it lacks chemical specificity and spatial resolution. In situ infrared microscopy can provide chemical specificity, but spatial resolution is only in the range of micrometers even at synchrotron facilities. In situ electrochemical X-ray absorption spectroscopy[20] is chemically sensitive, but implementations to date do not provide spatial resolution beyond the size of the synchrotron beam, typically 1 mm. In situ electrochemical X-ray standing wave[21] and X-ray reflectivity techniques[18] are very powerful tools to unravel subtle changes in the top few atomic layers of an electrode and the adjoining electrolyte layer. However, well-characterized and almost defect-free single-crystal surfaces are required, so these techniques are not generally applicable to the polycrystalline, and typically rough surfaces of most electrodes. In addition, unless used in a resonant mode,[22] reflectivity techniques do not provide chemical sensitivity, and they do not have lateral spatial resolution.

While the main thrust of this work is development of the instrumentation and techniques for in situ electrochemical STXM, we also wished to apply it to a relevant system. Electrochromism, the reversible change in optical properties of a material when it is electrochemically oxidized or reduced, is of great academic and commercial interest.[23] An important class of electrochromic materials is conducting polymers, thin films of which are being developed for display[6,7] and "smart window" applications.[24] Polyaniline (PANI) has been studied extensively in recent years for its potential use in electrochromic devices.[25] It is generally agreed that PANI exists in three well-defined oxidation states: leucoemeraldine, emeraldine, and pernigraniline. Fully reduced leucoemeraldine is a yellowish compound, while fully oxidized pernigraniline is dark purple. Both leucoemeraldine and pernigraniline have lower conductivity than emeraldine. Conducting emeraldine salt (green) is obtained from partial oxidation of leucoemeraldine (or partial reduction of pernigraniline) in aqueous protonic acids. Emeraldine base (blue) is formed from the salt in neutral or basic solution, without any change in the number of electrons. Emeraldine base is 9−10 times less conducting than emeraldine salt. Proton doping of emeraldine base is the first well-established example of the conversion of an organic polymer to a highly conducting regime by a chemical doping process in which the number of electrons associated with the polymer remains unchanged.[25] The proposed chemical structures of these states are given in Chart 1. It is noteworthy that the exact chemical structures involved at the various stages of the redox transformations of polyaniline are not fully characterized, and thus, the spectroscopic results of this study may contribute to further elucidation of these structures. The most stable PANI electrochromic devices use a restricted potential range, to allow only the yellow and green states to be formed.[26] The microstructure, and thus the performance of the resulting film, depends to a large degree on the method used to prepare the polymer.[27,28] Many factors such as electrolyte, pH, counteranion, and rate of deposition play a role in producing polyaniline of different morphologies, which affects the performance of the electrochromic device in terms of its switching speed, efficiency, etc. In addition, the transition rate and degree of completeness of the transformations

Chart 1. Proposed Chemical Structures of Polyaniline (PANI) in Various Chemical States[25]

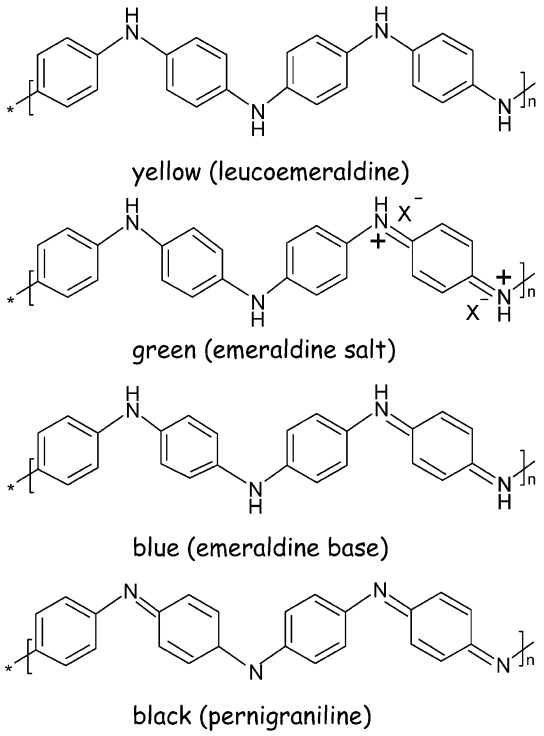

(14) Varma, R., Selman, J. R., Eds. *Techniques for Characterization of Electrodes and Electrochemical Processes*: Wiley: New York, 1991.
(15) Hamnett, A.; Abel, A.; Eameaim, J.; Christensen, P. A.; Timonov, A.; Vasilyeva, S. *Phys. Chem. Chem. Phys.* **1999**, *1*, 5147−5157.
(16) Kim, J. W.; Lee, J. Y.; Park, S. M *Langmuir* **2004**, *20*, 459−466.
(17) Balasubramanian, M.; Sun, X.; Yang, X.-Q.; McBreen, J. *J. Power Sources* **2001**, *92*, 1−8.
(18) Herrero, E.; Buller, L. J.; Li, J.; Finnefrock, A. C.; Solomón, A. B.; Alonso, C.; Brock, J. D.; Abruña, H. D. *Electrochim. Acta* **1998**, *44*, 983−992.
(19) Chabanier, C.; Guay, D. *J. Electroanal. Chem.* **2004**, *570*, 13−27.
(20) Alves, M. C.; Watanabe, N.; Ramos, A. Y.; Tolentino, P. *J. Synchrotron Radiat.* **2001**, *8*, 517−519.
(21) Zegenhagen, J.; Materlik, G. *Synchrotron Radiat. News* **1993**, *6*, 19−22.
(22) Hodeau, J.-L.; Favre-Nicolin, V.; Bos, S.; Renevier, H.; Lorenzo, E.; Berar, J.-F. *Chem. Rev.* **2001**, *101*, 1843−1868.
(23) Rowley, N. W.; Mortimer, R. J. *Sci. Prog.* **2002**, *85*, 243−262.
(24) Rauh, R. D. *Electrochim. Acta* **1999**, *44*, 3165−3176.
(25) Gospodinova, N.; Terlemezyan, L. *Prog. Polym. Sci.* **1998**, *23*, 1443−1459.
(26) Choi, S. J.; Park, S. M. *J. Electrochem. Soc.* **2002**, *149*, E26−E34.
(27) Zhou, H. H.; Jiao, S. Q.; Chen, J. H.; Wei, W. Z.; Kuang, Y. F. *Thin Solid Films* **2004**, *450*, 233−239.
(28) Reemts, J.; Parisi, J.; Schlettwein, D. *Thin Solid Films* **2004**, *466*, 320−325.

among the various states of PANI are known to be strongly affected by the electrochemical procedures used.[25]

Here we have used the interconversion of an electrodeposited polyaniline layer between the yellow leucoemeraldine (reduced) and the green emeraldine chloride (oxidized) states as a test platform to demonstrate in situ electrochemical STXM. The NEXAFS spectra of the yellow and green forms of PANI generated ex situ, along with the spectra of a concentrated solution of aniline in 1 M HCl, are first presented and discussed in detail. Then, in situ images, spatially resolved spectra, and chemical-state maps of the system in various electrochemical states are presented. In addition, we demonstrate in situ electrochemical studies time coincident with the spectromicroscopy on a subsecond time scale.

EXPERIMENTAL SECTION

The interferometrically controlled scanning transmission X-ray microscope[29] at bending magnet beamline 5.3.2 [30]at the Advanced Light Source (ALS) was used. The methods of measuring and analyzing STXM images and spectra have been described elsewhere.[8,9] The aXis2000 program[31] was used to process the spectral and image data.

The electrochemical cell was constructed from two 1.5 × 1.5 mm X-ray translucent silicon nitride windows[32] formed in a 200-μm-thick, 7.5 × 7.5 mm Si wafer frame (Figure 1). One of the windows was coated with multiple pads of electrically isolated, 10- or 20-nm Au thin film, which was used as the substrate. A two-electrode system was employed in the experiment, with one Au pad as the working electrode and the other Au pad as the counter electrode. A thin film of polyaniline of variable thickness (100−500 nm) was formed on the Au working electrode by a 10−15-s electrodeposition from a solution consisting of 0.1 M aniline in 1 M HCl using standard procedures.[25,33] Aniline was purchased from Aldrich and was purified by vacuum distillation prior to use. PANI was deposited ex situ. As indicated by a visual inspection of the working electrode and the marked increase of the current, polymer deposition on the working electrode occurs at potentials larger than 1.0 V (two-electrode configuration). For comparison, under the same experimental conditions, polymer deposition occurs at a potential of +0.85 V versus a Ag/AgCl reference electrode in a three-electrode setup. The ex situ deposition was carried out for 10−60 s, until the integrated current was such that ~500 μC flowed, generating ~10^4 μm^3 of PANI (a nonuniform deposit approximately 300 × 300 × 0.2 micrometers in size). After electrodeposition, the coated window was rinsed multiple times with deionized water to remove unreacted aniline and any nonadhering flakes of polyaniline. It was then air-dried.

The reference spectra (emeraldine chloride and leucoemeraldine) were obtained from samples made by electrodeposition of PANI on a Au-coated Si wafer and set to the oxidized or reduced forms by adjusting the potential. Parts of the PANI film flaked off and were transferred to a standard transmission electron microscopy Cu grid. When in situ measurements were planned, a wet cell was constructed by covering the dried PANI film, previously prepared by electrodeposition as described above, with a thin (~1 μm) overlayer of 1 M HCl by placing a ~1−2-μL drop (minimum deliverable from an Eppendorf pipet) and using the corner of a piece of lens paper to remove 80−90% of that drop. The area of the wet cell is 10 mm × 10 mm (of which only 1.5 mm × 1.5 mm is the X-ray transparent region; the remainder being 200-μm-thick silicon wafer), so a uniform 1-μm electrolyte film corresponds to a volume of 0.1 μL. Any excess HCl solution flows outside the boundaries of the top window when the wet cell is completed by placing a second silicon nitride window (without Au electrodes), with its window area aligned with the Au electrode-coated window. The wet cell was then sealed with 5-min epoxy (Hardman), and in some cases, a thin layer of a silicone vacuum grease (Dow Corning) was placed at the junction of the two window frames to ensure a complete water seal. The electrical connections to the cell were made by leaving a few hundred micrometers of the Au thin-film electrodes exposed on one side of the wet cell. Stainless steel spring clips were then used to contact those regions of the Au film (see Figure 1). A small amount of conducting Ag epoxy was used to ensure reliable electrical contact between the spring clip and the Au film. Prior to being installed into the STXM, the cell was tested outside the STXM to ensure proper contact and nonohmic behavior. Electrical connection to the tops of stainless steel spring clip electrodes completed the circuit, allowing a potential to be applied from outside the microscope during STXM measurements. All electrochemical reactions were controlled and monitored by a Pine instrument model RDE4 potentiostat operated in single-channel mode. A PMD-1208LS interface module (Measurement Computing) operated from LabView (version 7.0) was used to collect data from the potential and current monitors of the potentiostat. For time-dependent measurements, the potential was acquired simultaneously by the STXM acquisition program in order to correlate electrochemical and spectroscopic changes with a timing accuracy of a few milliseconds.

It was possible in favorable cases to operate some of the electrochemical wet cells through as many as 15 cycles. However, in many cases irreversible changes occurred, typically leading to loss of electrical contact with the film, either because the Au layer deadhered or fractured or because the HCl electrolyte solution displaced from the film, probably due to gas (H_2 and O_2) evolution from the reduction and oxidation of electrolyte on the counter electrode due to overpotential conditions. Different solutions are being sought to overcome these problems. A Cr adhesion layer and thick (200 nm) Au contact strips in the center of the X-ray transparent regions (5 nm Cr, 15 nm Au) are being used for our next generation of window substrates to improve adhesion of the Au to the Si_3N_4 surface, improve electrical conductivity, and reduce the probability of failure by fracture or deadhesion of the Au. In an attempt to avoid gas evolution, we deposited PANI on both working and counter electrodes (electrically isolated 10-nm-thick Au pads on the same window). However, four attempts to use this approach all lead to cells that failed after one full potential cycle (−1.1 to 1.1 V); i.e., no more electrical current could be

(29) Kilcoyne, A. L. D.; Tylisczak, T.; Steele, W. F.; Fakra, S.; Hitchcock, P.; Franck, K.; Anderson, E.; Harteneck, B.; Rightor, E. G.; Mitchell, G. E.; Hitchcock, A. P.; Yang, L.; Warwick, T.; Ade, H. *J. Synchrotron Radiat.* **2003**, *10*, 125−136.

(30) Warwick, T.; Ade, H.; Kilcoyne, A. L. D.; Kritscher, M. Tylisczcak, T.; Fakra, S.; Hitchcock, A. P.; Hitchcock, P.; Padmore, H. A. *J. Synchrotron Radiat.* **2002**, *9*, 254−257.

(31) aXis2000, written in Interactive Data Language (see www.rsinc.com), is freeware available at http://unicorn.mcmaster.ca/aXis2000.html.

(32) Silson Ltd. JBJ Business Park, Northampton Rd., Blisworth, Northampton, England, NN7 3DW.

(33) Adams, P.; Laughlin, P. J.; Monkman, A. P.; Kenwright, A. M. *Polymer* **1996**, *37*, 341−3417.

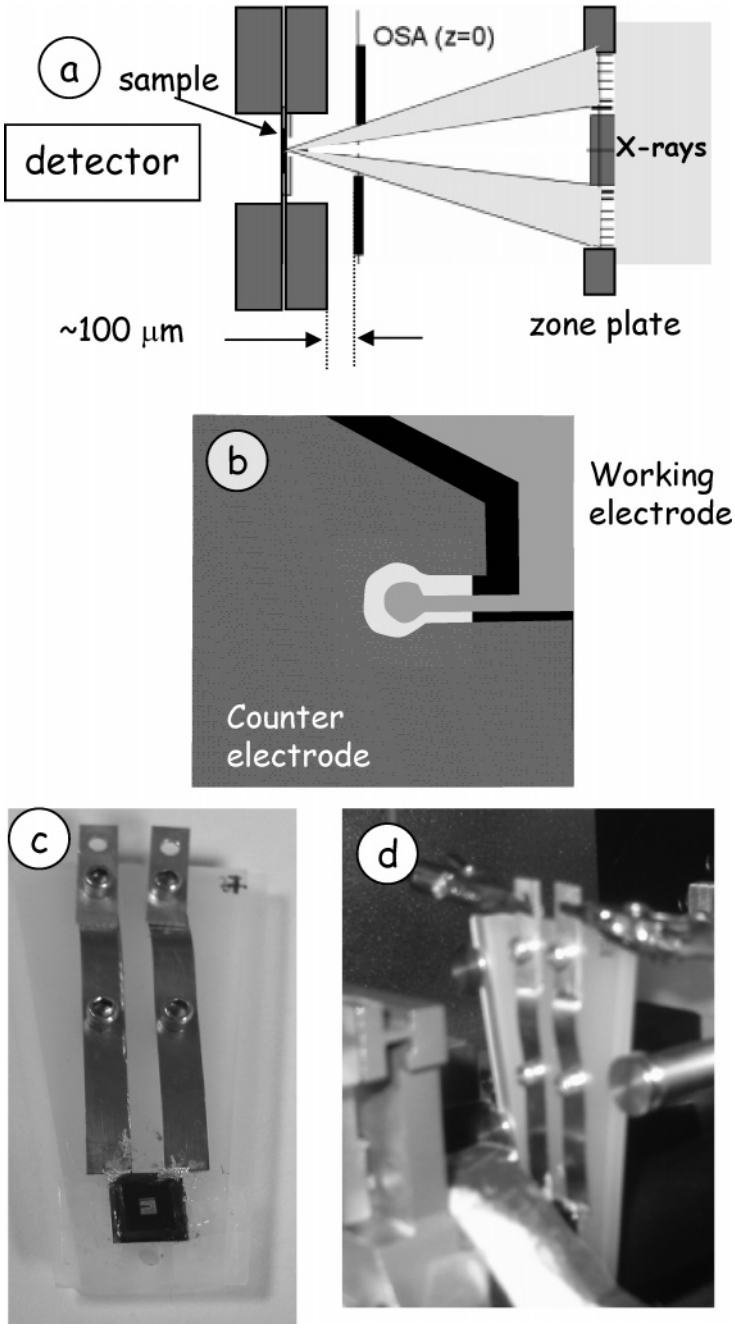

Figure 1. (a) Schematic of key elements of STXM. (b) Pattern of Au electrodes (10-nm thickness) on a silicon nitride membrane window (1500 × 1500 μm, 75 nm thick) in a Si wafer used for in situ electrochemical STXM. (c) Photograph of the sample holder. Electrical contacts are stainless steel spring clips; ridges on the side of the poly(chlorotrifluoroethylene) body provide kinematic relocation of the sample relative to the X-ray beam. (d) Photograph of the holder in beamline 5.3.2 STXM at the ALS.

passed through the cell. STXM images revealed a narrow line of inorganic substance on the edge of the electrode after the cell failed. One possible explanation could be Au curling up at the edge of the electrode due to disruption of the Au layer from dimensional change of the polyaniline during oxidation and reduction reactions. Windows with better Au adhesion through use of a few nanameter Cr interlayer and a slightly thicker Au layer (15 versus 10 nm) will be used in the future to reduce this factor.

RESULTS AND DISCUSSION

Imaging and Spectroscopy. The morphology and electronic structure of polyaniline prepared ex situ in the oxidized (green) and the reduced (yellow) forms were studied by STXM. An optical density image of the PANI sample (green form) recorded at 285.2 eV is shown in Figure 2. Very fine fibers (~50-nm diameter) are observed, similar to the morphology obtained by Choi and Park and visualized by scanning electron microscopy.[26]

Figure 3 presents the C 1s and N 1s NEXAFS spectra measured for a concentrated aniline/HCl solution (0.05 M aniline in 1 M HCl) and the leucoemeraldine (reduced) and emeraldine chloride (oxidized) forms of PANI. The energies and proposed assignments for the spectral features of all three species are summarized in Table 1, along with spectral information from the literature,[34] which reported the NEXAFS spectra of condensed

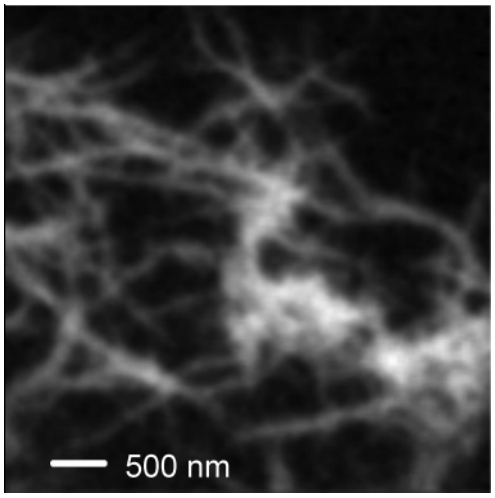

Figure 2. Image of dry polyaniline, recorded with STXM at 285.2 eV. The as-recorded transmission signal has been converted to optical density.

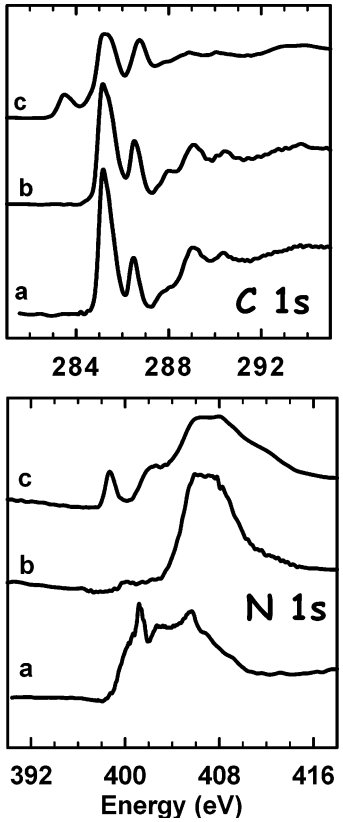

Figure 3. C 1s and N 1s X-ray absorption spectra of (a) 5% solution of aniline in 1 M HCl in a wet cell, (b) leucoemeraldine (yellow), and (c) emeraldine chloride (green), recorded with STXM. The PANI samples were free-standing dry thin films, transferred from a Au-coated Si electrode to a 3-mm Cu grid.

aniline, polyaniline as the emeraldine base prepared by a chemical route, and several proton doped states of the emeraldine base. The materials studied in ref 34 are all in the same oxidation state. In contrast, in this study we have investigated the electronic structure of PANI in different oxidation states (leucoemeraldine and emeraldine chloride).

Table 1. Energies and Proposed Assignments of the C 1s and N 1s Spectral Features of an Acidic Aniline Solution, Leucoemeraldine and Emeraldine Chloride[a]

(A) 5% Aniline Solution, Leucoemeraldine

energy (±0.1 eV)			proposed assignment	
aniline (aq)	leuco-emeraldine	lit.[34]	C−H	C−N
C 1s				
285.2	285.2	285.5	$1\pi^*$	
286.5	286.6	286.8		$1\pi^*$
288.0	288.0	288.0	σ^*_{C-H}	
289.1	289.1	289.2	$2\pi^*$	
290.4	290.4	290.7		$2\pi^*$
294.0 (4)	294.0 (4)	294(1)	σ^*	σ^*
301.7 (4)	301.7 (4)	-	σ^*	σ^*
N 1s				
401.1	399.9 (w)	-	σ^*_{N-H}	
403.0	402.4 (sh)	-	σ^*_{N-H}	
403.5 (3) (br)	406.5 (3)	-	σ^*_{C-C}, σ^*_{C-N}	
405.6	-	-		
420.4 (6)	420.7 (6)	-	σ^*	

(B) Emeraldine Chloride

energy (±0.1 eV)	lit.[34]	proposed assignment C−H	proposed assignment C=N
C 1s			
283.6	284.2 (sh)		$\pi^*_{C=C}$ (quinoid)
285.2	285.4	$1\pi^*$	
286.7	286.6		$\pi^*_{C=N}$
287.9 (w, sh)	287.8 (sh)	σ^*_{C-H}	
288.7	288.8	$2\pi^*$	
290.4	290.3 (sh)		$2\pi^*$
294.0 (4)	293.0(6)	σ^*	σ^*
301.7 (4)	302.5(8) (w)	σ^*	σ^*
N 1s			
398.7	399.0	$\pi^*_{C=N}$	
402.4	404.0	$2\pi^*$ (?)	
407	409.3 (6)	$\sigma^*_{C=N}$	
421 (sh)	-	σ^*	

[a] w, weak; br, broad; sh, shoulder.

In the fully reduced form, the aromatic rings are all intact and thus the electronic structure of the ring carbons is expected to be quite similar to that of aniline, consistent with the strong similarity of the C 1s spectra of the aniline solution and leucoemeraldine. The π^* region of the spectra of both species is dominated by two strong, narrow features in a ~2:1 intensity ratio. The lower energy feature at 285.2 eV is the C 1s(C−H) → $1\pi^*_{ring}$ transition, while the higher energy peak, located at 286.5 eV in aniline solution, and 286.6 eV in leucoemeraldine, corresponds to the C 1s(C−N) → $1\pi^*_{ring}$ transition. At higher energy, there are weaker peaks at 289 and 290 eV which we attribute to C 1s-(C−H) → $2\pi^*$ and C 1s(C−N) → $2\pi^*$ transitions. [Nomenclature note: $1\pi^*$ refers to the unresolved combination of the a_2 and b_1 π^* states (using C_{2v} symmetry for aniline)[35] which correspond to the e_{2u} π^* state of benzene, while $2\pi^*$ refers to the b_1 state that corresponds to the b_{2g} π^* state of benzene.] At still higher energy, there are broad peaks at 294 and 302 eV corresponding to σ^*_{CC} states or resonances embedded in the C 1s ionization continuum. These features are very similar to those seen in a wide range of aromatic compounds.[35,36] The C 1s spectral features of the aniline

(34) Magnuson, M.; Guo, J.; Butorin, S.; Agui, A.; Sathe, C.; Nordgren, J.; Monkman, A. *J. Chem. Phys.* **1999**, *111*, 4756−4761.

(35) Turci, C. C.; Urquhart, S. G.; Hitchcock, A. P. *Can. J. Chem.* **1996**, *74*, 851−869.

solution and leucoemeraldine are similar to those of condensed aniline reported by Magnusson et al.,[34,37] although the latter spectrum was recorded at considerably lower energy resolution and there appears to be an error of ~0.3 eV in the energy scale. The energy scales of the spectra reported herein are accurate to 0.1 eV, based on calibration to CO_2 and N_2.

The N 1s spectrum of leucoemeraldine (Figure 3) does not have any strong, low-lying features. Rather, there is a weak broad band at ~400 eV, probably corresponding to N 1s → N−H transitions, and a strong broad band beginning at 403 eV and peaking at 406.5 eV, corresponding to N 1s → σ^*_{C-N} transitions, consistent with the saturated N environment in the reduced form. A second broad σ^* feature occurs at 420 eV (not shown in Figure 3). The two main broad peaks that dominate the N 1s spectrum of leucoemeraldine are also found in the N 1s spectrum of the aniline solution, although the lower σ^*_{C-N} resonance is shifted to lower energy and is overlapped by several sharp low-lying features in the aniline solution spectrum. We attribute the latter features to N 1s → σ^*_{N-H-O} transitions, associated with specific N−H−O conformations involved in hydrogen bonding between the NH_2 groups of aniline and water.

When the leucoemeraldine form of polyaniline is oxidized to form emeraldine chloride, a new, low-lying transition appears at 283.6 eV and there are small shifts and large intensity changes in other peaks in the C 1s spectrum. The 283.6-eV feature, which is associated with C 1s(C=C) → $\pi^*_{C=C}$ transitions in the quinoid ring, occurs at an energy similar to that found for the corresponding transition in hydroquinone.[38] The energy of the main C 1s-(C−H) → 1π^* transition is the same as that in leucoemeraldine, but its intensity decreases very significantly, consistent with conversion of a fraction of the aromatic rings to quinoid rings. The third peak at 286.7 eV is shifted 0.2 eV higher than its counterpart in leucoemeraldine, due to modification of the C 1s-(C−N) → 1π^* transition by the formation of C=N bonds. Structure in the 289−291-eV region, associated with C 1s → 2π^* transitions and C 1s → σ^*_{C-N} transitions, are also modified in intensity, although features are found at similar energies. There is little or no change in the high-energy continuum features associated with σ^* resonances. At the N 1s edge, there is a very dramatic change with the introduction of a strong, sharp feature at 398.7 eV associated with N 1s(C=N) → $\pi^*_{C=N}$ transitions. In addition there is a significant shift to higher energy in the strong, broad σ^*_{CN} peak, which is associated with shortening of the C−N bond.[13,39] Among all the spectral changes with oxidation, the new low-lying peaks at 283.6 and 398.7 eV are the clearest and thus they are the best suited to follow the electrochemical reaction.

In Situ Spectromicroscopy of Redox Modification of PANI. Polyaniline samples on the Au-coated Si wafer were modified in situ by changing the potential in either a discrete or a cyclic fashion in the range between +1.1 and −1.1 V while recording the current flow. Leucoemeraldine (yellow) was observed to undergo oxidation to the emeraldine chloride (green) at a potential near 0.8 V while the reverse reduction reaction happened at −0.5 V as indicated by the onset of peaks in the cyclic voltammogram (CV) (Figure 4). As noted in earlier work,[25] the reduction process is much slower and thus the reduction wave is less sharply peaked than the oxidative wave in the CV. In addition, there is a subsidiary current maximum around −0.1 V in both the anodic and cathodic scans.

To study in more detail the electronic structure and film morphology of the various electrochemical states, we held the system at selected potentials (at the points labeled in Figure 4) and recorded NEXAFS point spectra (X-ray absorption spectrum of a single location of the sample, selected by the user from a previous image) and images at several characteristic photon energies. In each case, the spectra were measured after the current flow had returned to zero. In the C 1s (Figure 5) and N 1s (Figure 6) regions, spectral changes characteristic of the expected oxidation and reduction changes are observed. However,

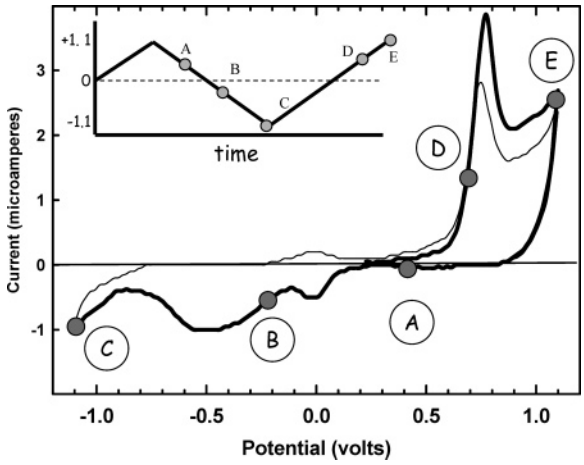

Figure 4. Two-electrode cyclic voltammetry of a PANI film recorded while the sample was being measured in the STXM. The inset shows the potential profile that was applied to the sample. The letters (A−E) indicate the selected potentials at which NEXAFS point spectra and images were recorded (see the next two figures).

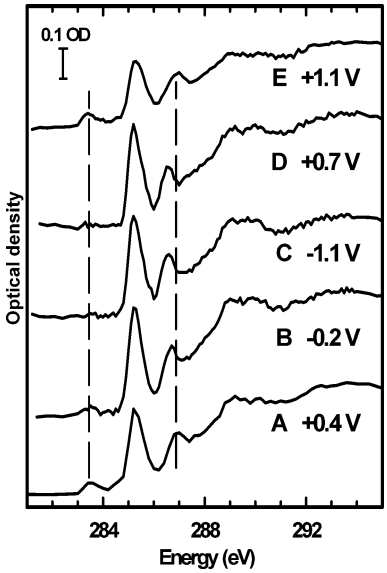

Figure 5. C 1s spectra of polyaniline at various potentials (see Figure 4) recorded at a single point, at the position indicated by the white circle in Figure 7. The dashed lines are guides to assist visualization of the key spectral changes.

(36) Horsley, J. A.; Stöhr, J.; Hitchcock, A. P.; Newbury, D. C.; Johnson, A. L.; Sette, F. *J. Chem. Phys.* **1985**, *83*, 6099−6107.
(37) Luo, Y.; Agren, H.; Guo, J.-H.; Skytt, P.; Wassdahl, N.; Nordgren, J. *Phys. Rev.* **1995**, *A 52*, 3730−3736.
(38) Francis, J. T.; Hitchcock, A. P *J. Phys. Chem.* **1992**, *96*, 6598−6610.
(39) F. Sette, F.; Stöhr, J.; Hitchcock, A. P. *J. Chem. Phys.* **1984**, *81*, 4906−4914.

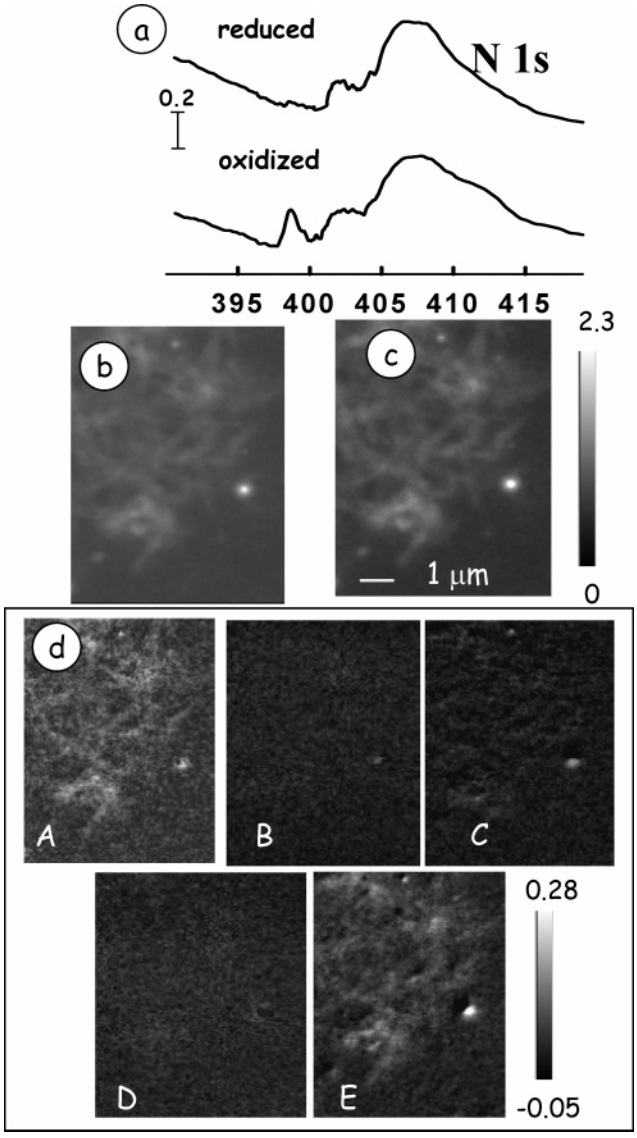

Figure 6. (a) N 1s spectra recorded in the oxidized (green) and reduced (yellow) states at the position indicated by the white circle in Figure 7. (b) Optical density images at 395 and (c) 398.7 eV of the sample in the reduced state (A). (d) Sequence of difference images [*I*(398.7 eV) − *I*(395 eV)] recorded at various potentials (see Figure 4). The gray scales beside the images and the bar in (a) indicate the optical density range.

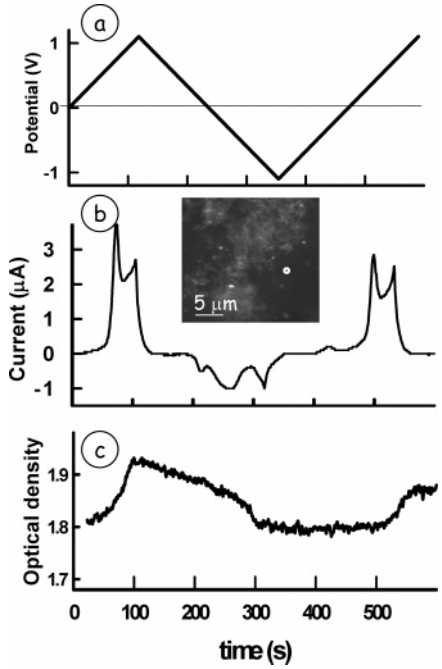

Figure 7. (a) In situ imposed potential variation on the sample. (b) Corresponding current flows. Inset: image at 285.2 eV of the region examined. The white circle is where the potential dependent spectra in Figures 5 and 6 were acquired. (c) Change in transmitted intensity at 283.6 eV (C 1s → π^*_{quinoid}) associated with the indicated current and potential changes.

the extent of change was diminished relative to that found when the emeraldine chloride was formed ex situ and studied spectroscopically (Figure 3). We interpret the much smaller changes in the in situ setup as indicating that only a portion of the material being sampled is undergoing reduction, either due to kinetic factors or due to loss of electrical contact. In more detail, the C 1s spectrum of the initially oxidized material (A) transforms almost but not completely to the reduced (yellow) form after passing through the first, small reduction peak at −0.1 V and being held at −0.2 V (B). Further reduction occurred when the potential was dropped to −1.1 V (C), to form the fully reduced state (leucoemeraldine). When the potential was then increased past the small peak at −0.1 V in the oxidative direction, negligible change in the spectrum was observed even when the potential had been increased to +0.7 V (D). It is only when the potential is increased to +1.1 V (E) that the material transforms to the green oxidized state, giving rise to a C 1s spectrum very similar to the initial one (A).

To visualize changes in film structure associated with electrochemical conversion in the electrochemical cycle, pairs of images were measured at 398.7 and 395 eV at the stationary points indicated by the lettered labels in Figure 4. Figure 6a plots the N 1s spectra recorded from a single point in the electrochemical cell, Panels b and c in Figure 6 are an example of the pair of images at state A, Figure 6d displays the difference in these images at all five stationary states. We refer to the difference images as "electrochemical imaging", since they only display that portion of the whole sample that is undergoing electrochemical change. The difference of the images at these two photon energies should reveal the portions of the film that are oxidized, since only the oxidized material will exhibit a peak at 398.7 eV. As expected, features are observed only in the difference images of states A and E (oxidized PANI). According to the intensity of the 398.7-eV feature seen in the point spectrum of oxidized PANI (Figure 6a), a ∼0.2 OD unit difference is expected in the difference image of a polymer having adjacent regions of differing activity. A comparison between the expected and measured image difference signal reveals that in states A and D basically the entire polymer is converted to the oxidized form. Imaging the electrochemically active and inactive components of an apparently uniform film is an example of the power of the electrochemical-STXM technique.

Probing Electrochemical Kinetics with Spectroelectromicroscopy Measurements. Figure 7 presents an example of in situ kinetic studies. Simultaneous with scanning the potential at a rate of 10 mV/s and recording the cyclic voltammogram, the intensity of the transmitted X-rays at 283.6 eV was measured with

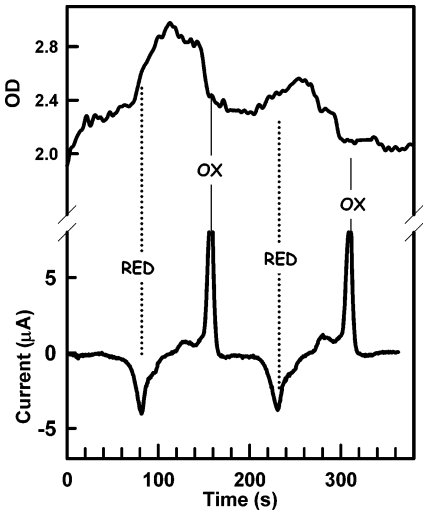

Figure 8. Time dependence of the change in optical density at 398.7 eV associated with potential changes obtained by measuring signal at a point with a 0.2-μm defocused beam, while changing the potential and measuring the current.

500-ms sampling. The optical density derived from the transmission signal is plotted in Figure 7c. It varied in a cyclic manner with a characteristic line shape that reflects the kinetics of the change in electronic structure as the polyaniline transforms between the quinoid and aromatic forms. In our first measurements, there was some possibility of radiation damage, since we used the focused beam in the STXM, which delivers a very high radiation dose rate. In later measurements, the beam was defocused to 0.2 μm in order to reduce the dose and thus the damage rate ~20-fold. Figure 8 shows results from a measurement in which 398.7-eV light passing through the indicated spot on a PANI thin film was monitored as the potential was cycled between 1.0 and −1.0 V for over a dozen cycles at a scan rate of 10 mV/s. The spectral response of that point in the PANI film was monitored, and changes on a subsecond scale were observed. The chemical changes monitored by NEXAFS were found to have a time-dependent form different from that observed for the current flow. Specifically the onset of the reduction in the NEXAFS spectrum began only at the *peak* of the current flow and extended over a period of time beyond the termination of the current flow. In contrast, the onset of the oxidation, as detected by a decrease in the OD at 398.7 eV, coincided with the onset of the oxidative current flow and terminated at the same time as the current flow terminated. While there is a characteristic asymmetry in the reduction step in the CV as well as the time/potential dependent NEXAFS, the temporal characteristics differ. The oxidation process happens at a faster rate than the reduction, as indicated by steeper slopes of the transmission and CV signals as the oxidation process turns on and completes.

The time dependence of the reduction process was also sampled not just at a single point on the sample but also over an extended line, thus sampling portions of the PANI sample that might have different electrochemical characteristics. Figure 9 plots the results from a line scan measurement in which successive passes over a 24-μm-long line on the sample were recorded as the potential was changed with the X-ray energy fixed at 398.7 eV. The X-ray beam was defocused to 0.2 μm for this measurement. Note that the last 10% of the line actually extends off the

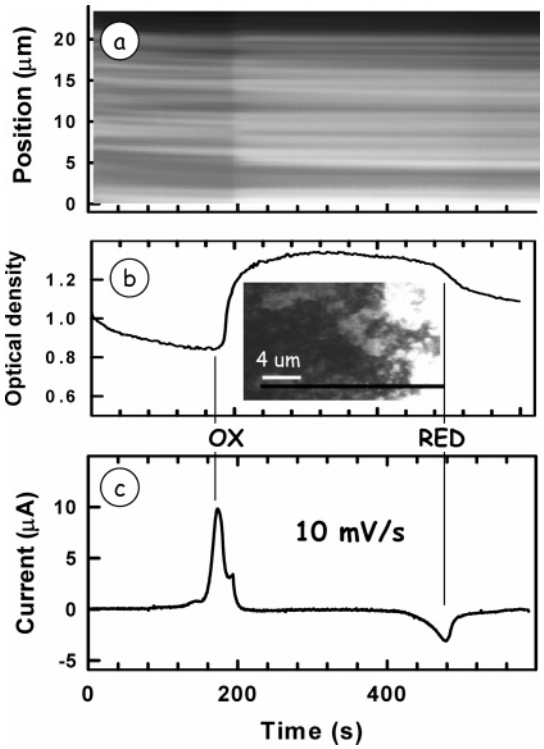

Figure 9. (a) Time dependence of the optical density at 398.7 eV along a 24-μm line associated with the indicated current changes associated with scanning the potential (10 mV/s) from 0 up to +1.1 V, back to −1.1 V, and then to 0 V (see Figure 7a). The X-ray beam was defocused to 0.2 μm. (b) Integrated optical density changes as a function of time/potential. The inset shows the position of the line scan on the sample. Note the rightmost ~3 μm is not on the Au electrode yet spectral changes with potential are detected. (c) Time-dependent current flow.

Au contact film, and yet there is detectible electrochemical reaction as indicated by the abrupt change in OD at the 190-s point. The 398.7-eV peak grows in visibility slightly after the maximum in the oxidative current but disappears slowly on the reduction step. This is a clear indication there is a large difference in the kinetics of the oxidation and reduction processes, not just on a spatially averaged but also on a point-by-point basis. This observation is consistent with other, nonspatially resolved observations, which are discussed at length in the review by Gospodinova and Terlemezyan.[25] While our work to date does not provide specific insights into the reasons for the differences in the oxidation and reduction kinetics, the development of the novel tool of in situ electrochemical STXM provides a new, spatially resolved chemical spectroscopy under potential control, which holds promise to contribute to unraveling the complexities of the electrochemical processes in polyaniline and other conducting polymer thin films. Furthermore, in situ electrochemical STXM can be performed on a point-by-point basis at millisecond time scales. This is the relevant time domain to help understand this, and other systems such as organic display systems where chemical form, molecular orientation, or both are changed by an applied potential.

SUMMARY

Scanning transmission X-ray microscopy has been applied for the first time to track in situ electrochemical changes. The

morphology, chemical state, and kinetics of the redox chemistry were monitored by STXM imaging and spatially resolved NEXAFS spectroscopy over multiple electrochemical cycles which alternatively oxidized and reduced a thin, spaghetti-like film of polyaniline. The spatial resolution in these measurements was ~50 nm, and changes were observed on a subsecond time scale. The rate of the temporal changes was limited by the properties of the chemical system, not the ability of STXM to make measurements, as point measurements with a few percent statistical precision can be made with millisecond sampling. The work reported herein fulfills the goals of the initial phase of this project, which was to develop the techniques and apparatus and to demonstrate that in situ electrochemical STXM is possible. Improvements in experimental design will make the system more robust and adaptable to a wide range of systems, including the direct study of the redox interaction between PANI and other molecules (sensor technology). We plan to extend the technique to studies of planar multilayer structures with transverse fields, such as those common in display, fuel cell, and battery applications. In situ electrochemical STXM will be applicable to any system for which one can prepare a sample that incorporates the relevant parts of the scientific problem, with adequate X-ray transparency at the core excitation edge of interest. For C 1s studies, this means a total path length of organic material of less than 200 nm, with all other components contributing no more than 1.5 optical density units. In our case, this criterion is met with our system, which consists of ~1 μm of water, 20 nm of Au, 150 nm of Si_3N_4, and ~150 nm of polyaniline. For studies at higher energy edges (e.g., N 1s ~ 400 eV, metal 2p edges in the 600−900-eV range), the spatial constraints are considerably relaxed. Since soft X-ray STXM can be performed using undulator beamlines up to 2 keV, and there are STXM devices covering the full range of X-ray energies, it should be possible in favorable cases to make useful, chemically sensitive measurements on micrometer-thick layers. As interfaces between layers are a major concern, it is useful to note that we are already able to examine interface systems such as monolayer protein adsorption at the interface between 1 μm of protein solution and 100 nm of a multiphase polymer.[11]

ACKNOWLEDGMENT

This work is funded by the Natural Science and Engineering Research Council (Canada) and the Canada Research Chair program. The Advanced Light Source is supported by the Director, Office of Energy Research, Office of Basic Energy Sciences, Materials Sciences Division of the U.S. Department of Energy, under Contract DE-AC03-76SF00098. We thank David Kilcoyne and Tolek Tyliszczak for their expert development and maintenance of the ALS STXM532 facility. Zone plates used at the ALS were provided by the Centre for X-ray Optics, Berkeley Lab. We thank Peter Anastasi and Keith Vanner for assistance with design and for their expertise in fabricating the patterned Au-coated silicon nitride windows.

Received for review December 29, 2004. Accepted March 22, 2005.

AC048077J